(20) R. A. W. Johnstone, F. A. Mellon, and S. D. Ward, *Int. J. Mass Spectrom. Ion Phys.*, **5**, 241 (1970).
(21) W. C. Price, J. P. Teegan, and A. D. Walsch, *J. Chem. Soc.*, 920 (1951).
(22) J. E. Collin and R. Locht, *Int. J. Mass Spectrom. Ion Phys.*, **3**, 465 (1970).
(23) J. L. Franklin, J. F. Dillard, H. M. Rosenstock, J. T. Herron, K. Draxl, and F. H. Field, *Natl. Stand. Ref. Data Ser., Natl. Bur. Stand.*, **No. 26** (1969).
(24) S. W. Benson, F. R. Cruickshank, D. M. Golden, G. R. Haugen, H. E. O'Neal, A. S. Rodgers, R. Shaw, and R. Walsh, *Chem. Rev.*, **69**, 279 (1969).
(25) G. Wolf, *Helv. Chim. Acta*, **55**, 1446 (1972).
(26) R. L. Nuttall, A. H. Laufer, and M. V. Kilday, *J. Chem. Thermodyn.*, **3**, 167 (1971).
(27) R. N. Lacey, "The Chemistry of Alkenes", Patai, Ed., Interscience, London, 1964.
(28) F. Compernolle, *Org. Mass Spectrom.*, in press.
(29) JANAF Thermochemical Tables, D. Stull, Ed., Dow Chemical Co., Midland, Mich., 1965, Addenda 1966, 1967.
(30) H. Okabe, *J. Chem. Phys.*, **53**, 3507 (1970).
(31) Ju. A. Strepichejew, Ju. I. Baranow, and O. A. Burmisstrova, *Chem. Zentralbl.*, **136**, 15517 (1965).
(32) D. D. Wagman, W. H. Evans, V. B. Parker, I. Halow, S. M. Bailey, and R. H. Schumm, *Natl. Bur. Stand. (U.S.), Tech. Note*, **No. 270-3** (1968).
(33) P. Lemoult, *C. R. Hebd. Seances Acad. Sci.*, **126**, 43 (1898).
(34) M. A. Haney and J. L. Franklin, *J. Chem. Phys.*, **48**, 4093 (1968).
(35) J. G. Dillard and J. L. Franklin, *J. Chem. Phys.*, **48**, 2353 (1968).
(36) J. L. Franklin, V. H. Dibeler, R. M. Reese, and M. Krauss, *J. Am. Chem. Soc.*, **80**, 298 (1958).
(37) T. F. Fagley and H. W. Myers, *J. Am. Chem. Soc.*, **76**, 6001 (1954).
(38) W. A. Roth and F. Müller, *Chem. Ber.*, **62**, 1190 (1929).
(39) P. D'Amario, G. Di Stefano, M. Lenzi, and A. Mele, *J. Chem. Soc., Faraday Trans. 1*, **68**, 940 (1972).
(40) R. G. Cooks, M. Bertrand, J. H. Beynon, M. E. Rennekamp, and D. W. Setser, *J. Am. Chem. Soc.*, **95**, 1732 (1973).
(41) J. H. Beynon, M. Bertrand, and R. G. Cooks, *Org. Mass Spectrom.*, 7, 785 (1973).
(42) E. Testa and L. Fontanella, *Justus Liebigs Ann. Chem.*, **660**, 118 (1962).
(43) E. Testa, L. Fontanella, G. F. Cristiani, and L. Mariana, *Helv. Chim. Acta*, **42**, 2370 (1959).
(44) A. Ebnöther, E. J. Jücker, E. Rissi, J. Rutschmann, E. Schreier, R. Steiner, R. Süess, and A. Vogel, *Helv. Chim. Acta*, **42**, 918 (1959).

Electrolyte-Induced Phase Transitions in Micellar Systems. A Proton and Carbon-13 Nuclear Magnetic Resonance Relaxation and Photochemical Study[1]

K. Kalyanasundaram, M. Grätzel, and J. K. Thomas*

Contribution from the Department of Chemistry and Radiation Laboratory, University of Notre Dame, Notre Dame, Indiana 46556. *Received October 15, 1974*

Abstract: The electrolyte-induced phase transition from spherical to rod-shaped aggregates in aqueous micellar solutions of dodecylammonium chloride (DAC) has been studied by means of proton and ^{13}C NMR and photochemical techniques. The shape of the proton NMR spectrum is changed drastically upon the addition of the electrolyte (broadening of the resonance lines and a drop in the intensity of the lines). The relative efficiencies of various anions in inducing the transition were found to follow the lyotropic series $Cl^- < Br^- = NO_3^- < ClO_4^-$. The relaxation times or T_1 values for different protons of the DAC molecule are not as greatly affected by the structural changes. The ^{13}C spectrum does not change significantly. T_1 values for backbone carbons (C_2 to C_9) are reduced, that of the α carbon is increased, and those of C_{10} to C_{12} remain unaffected upon the formation of rod-shaped aggregate. The dynamics of pyrene monomer and excimer fluorescence in the two structural forms was investigated by 347.1 nm ruby laser photolysis. The pyrene excimer yield depends both on the distribution of pyrene among the micelles and their rate of diffusion. In rod-shaped aggregates the diffusion occurs along the longitudinal axis of the rod with a rate which is about 2.5 times smaller than in a spherical micelle. The permeability of the spherical and rod-shaped micelles with respect to various species was studied by a kinetic analysis of the quenching of pyrene monomer fluorescence. Differences in the quenching efficiencies observed for ionic quenchers reflect a decreased surface charge in the rod-like structures. Quenching experiments with Br^- counterions yield an effective half-lifetime for the radial diffusion of the probe from the center to the periphery of the rods. Finally fluorescence depolarization studies using 2-methylanthracene and 1-anilino-8-naphthalenesulfonate as probes are reported. The former indicates a considerable increase in microviscosity of the micellar interior upon the formation of rods while the latter reveals no significant changes in the micellar surface region.

Micellar systems provide useful structural and functional models for more complex bioaggregates.[2] Possible analogies between micellar catalysis and enzyme catalysis have also been suggested.[3] Recently several interesting features of micellar assemblies have been established by the use of physicochemical techniques such as NMR[4] (chemical shift analysis as well as relaxation studies), ESR nitroxide[5] spin labeling, and fluorescent probe analysis.[6] While at relatively low concentrations surfactant molecules are associated in spherical micelles, other structural forms such as rods or bilayers occur in more concentrated solution.[7] A schematic illustration of such molecular organizations is presented in Figure 1. Similar structures can be produced, alternatively, by the addition of electrolytes.[8] Large micelles with a rod-like shape or bilayers are probably more suitable models for biomembranes. Hence a study of the formation and properties of these structures should provide some clues on the forces that govern the hydrophobic interactions in biological systems and also would lead to a better understanding of complex processes exhibited by these systems such as polymorphisms (thermotropic and lyotropic) and micellar catalysis of organic reactions.

The present investigation is directed toward an analysis of the electrolyte-induced sphere-rod transitions in surfactant solutions. Typical systems where these type of transitions occur are summarized in Table I together with literature data on the micellar shape and aggregation numbers. Of these dodecylammonium chloride/sodium chloride [abbreviated hereafter as DAC/NaCl] was selected as a suitable model system for detailed study. Several techniques were employed to monitor changes in the dynamic and static properties of the micellar assemblies, associated with the transition.

In the first part of the paper ^1H and ^{13}C NMR results are presented to characterize the sphere-rod transition. While a line-shape analysis of the proton and carbon-13

Table 1. Literature Data on the Aggregation of Micelles in the Presence of Electrolytes

Surfactant[a] and its concn (*M*)	Electrolyte and its concn (*M*)	Micellar shape	Micellar mol wt (Mmw)	Aggr No.	Temp, °C	Ref
DAC (<cmc)			222	1	35	8a
DAC (0.1)		Spherical	17,800	82	35	8a
DAC (0.1)	NaCl (0.1)	Rod shaped	85,500	~400	35	8a
DAC (0.1)	NaCl (0.2)	Rod shaped	655,000	≅3000	35	8a
DAC (0.1)	NaCl (0.25)	Rod shaped	1,125,000	≅5000	35	8a
DAC (0.1)	NaCl (0.3)	Rod shaped	1,800,000	≅7500	35	8a
DTAC (<cmc)			264	1	23	8a
DTAC (0.1)		Spherical	9,900	~35	23	8a
DTAC (0.1)	NaCl (0.1)	?	16,800	~65	23	8a
TTAC (<cmc)			292		23	8a
TTAC (0.1)		Spherical	10,100	30	23	8a
TTAC (0.1)	NaCl (0.1)	?	25,500	~80	23	8a
CTAB (<cmc)			365	1		8e
CTAB (0.1)		Spherical	29,000	~80		8e
CTAB (0.1)	NaBr (0.178)	Rod shaped	795,000	≅2000		8e
CTAB (0.1)	NaBr (0.233)	Rod shaped	1,860,000	≅4500		8e
CPC (<cmc)			338	1	31	8g
CPC (0.1)		Spherical	27,200	~80	31	8g
CPC (0.1)	NaCl (0.3)	Spherical	46,000	~135	31	8g
Hyamine 1622 (<cmc)			466	1	30	8c
Hyamine (<cmc) (0.1)		Spherical	6.25×10^3	14	30	8c
Hyamine (<cmc) (0.1)	NaCl (0.11)	Rod shaped	1.23×10^5	250	30	8c
Hyamine (<cmc) (0.1)	NaCl (0.30)	Rod shaped	7.25×10^5	1550	30	8c

[a] DAC = dodecylamine hydrochloride, DTAC = dodecyltrimethylamine hydrochloride, TTAC = tetradecyltrimethylammonium chloride, HDTAB = hexadecyltrimethylammonium bromide, CTAB = cetyltrimethylammonium bromide, CPC = cetylpyridinum chloride, hyamine 1622 = diisobutylphenoxyethoxyethyldimethylbenzylammonium chloride.

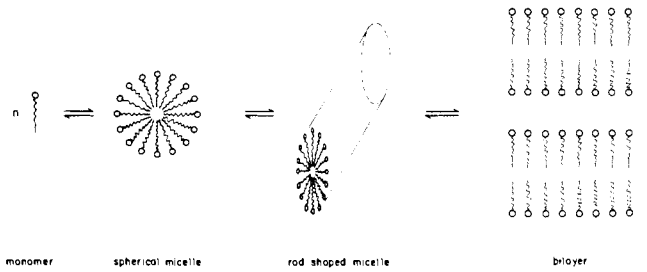

Figure 1. Different structural forms assumed by surfactant molecules in aqueous solutions.

spectrum reveals gross features of the process, a more detailed picture on the motility changes of the hydrocarbon tails of the surfactant molecules is obtained through spin-lattice relaxation time (T_1) measurements. Subsequently, a comparative study of the dynamic properties of spherical and rod-shaped micelles, through the use of fluorescent probes such as pyrene and 2-methylanthracene, is presented. The yields of pyrene monomer and excimer fluorescence coupled with a kinetic analysis of the fluorescence-time curves give information on the lateral diffusion of pyrene within the rod. Furthermore, the dynamics of pyrene fluorescence quenching elucidates the permeability of the micelle or rod-water interface with respect to various nonionic and ionic quenchers. Finally, evidence for a substantial increase in viscosity of the interior of micellar aggregates upon formation of rods, derived from fluorescence depolarization studies, is presented.

Experimental Section

Apparatus and Methods. High resolution ^1H, ^{13}C NMR spectra and T_1 measurements were carried out with a Varian XL-100 NMR spectrometer equipped with Nicolet TT-100 fourier transform accessories. All spectra were recorded in D_2O as solvent and at ambient probe temperature (≃35°). The samples were equilibrated in the probe for at least 10 min before each run. For calibration work, a 3% solution of TMS in $CDCl_3$ was used. The instrument operates at a frequency of 100.1 MHz for ^1H and at 25.2 MHz for ^{13}C and was locked onto the deuterium in the solvent.

The proton and proton-decoupled ^{13}C spectra were obtained on a fourier transform (FT) mode using pulsed rf power. The pulsewidth had a duration of 30 and 20 μsec for ^{13}C and ^1H measurements, respectively, and a time interval of 2 sec was used between two subsequent pulses to allow for recovery to equilibrium. An identical number of scans (8192) were accumulated to compare the line widths and intensities for various added electrolyte concentrations. The inversion recovery method of Freeman and Hill[9] involving a $(\pi\text{-}t\text{-}\pi/2)$ sequence (where t is the delay) was used to measure the T_1 values and the $\pi/2$ pulse had a duration of 52 and 22 μsec for ^{13}C and ^1H, respectively. The program samples 8192 data points on each FID (for a sweep width of 1000 Hz for proton and 2500 Hz for carbon-13) and typically 50 (for ^1H) and 1024 (for ^{13}C) scans were accumulated before fourier transformation. Higher numbers of scans were used on increasing the concentration of NaCl in order to achieve a better S/N ratio. All ^{13}C T_1 values were measured with proton-decoupled natural abundance ^{13}C PRFT spectra.

Laser photolysis studies were carried out with a KORAD frequency-doubled Q-switched ruby laser. The 347.1 nm laser pulse had a width of 15 nsec with an energy output of ≃200 mJ. Transient absorption and fluorescence were detected by means of fast kinetic spectroscopy, a detailed description of which has been given elsewhere.[10]

Steady state fluorescence and fluorescence depolarization studies were made on an Aminco-Bowman spectrophotofluorimeter. Suitable cutoff filters were placed on the excitation and emission channels to minimize the scattered light. Polacoat 105 polarizers with a spectral range of 200 to 800 nm were used to measure the degree of polarization. The experimental details for measuring the degree of polarization and the necessary equations which give microviscosity from the measured degree of polarization have also been described earlier.[6c] The concentrations of solubilized probes were measured from their absorption spectra recorded on a Cary 14 spectrophotometer.

Materials. DAC (Eastman) sample was recrystallized several times from alcohol–ether mixtures. All the *electrolytes* [NaCl, NaBr, NaI, $TlNO_3$, $CuCl_2$, $NaClO_4$] were of A.R. grade and were used as supplied.

Pyrene (Kodak) was passed through silica gel in cyclohexane solution and then recovered.

D_2O (Merck & Co., 99.9%) was used as supplied. Laboratory distilled water was redistilled from $KMnO_4$.

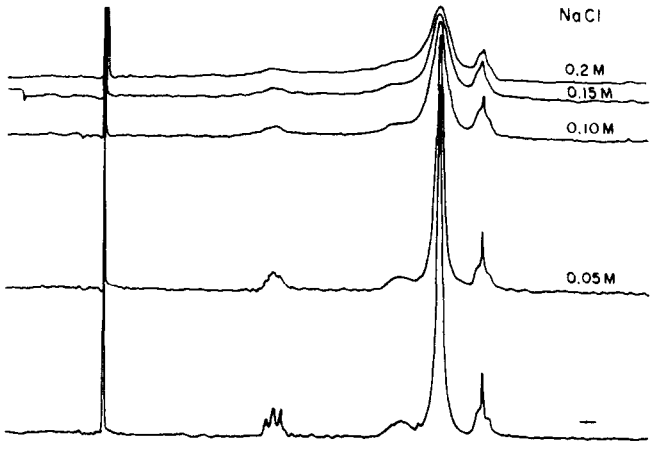

Figure 2. Effect of added NaCl on the ^1H NMR spectrum of micellar DAC (0.1 *M*) solutions in D_2O.

NMR Studies on DAC–NaCl Sphere–Rod Transition

(1) Proton NMR Studies of DAC–NaCl Solutions. The electrolyte-induced phase transition of spherical DAC micelles into rod-like structures has been investigated earlier by means of light scattering and viscosity measurements.[8a] While these techniques reveal changes in the shape and aggregation number of the micellar assemblies as a whole no detailed information can be derived regarding any possible changes in the dynamic properties of the hydrocarbon chains of the surfactant molecules which may occur during the phase transition. Nuclear magnetic resonance studies provide a very effective method for the investigation of the micellar solutions. Changes in the line width and spin–lattice relaxation times give information concerning the relative mobility of the particular grouping within the two different phases.

Figure 2 shows ^1H NMR spectra of 0.1 *M* DAC solutions in the absence and in the presence of increasing amounts of electrolyte, NaCl. The proton spectrum of DAC consists of five peaks: the H–OD resonance (at δ 4.95), the NH_3^+ triplet (centered δ 3.37), a strong CH_2 resonance (at δ 1.65) with the α-CH_2 appearing as a shoulder on the low field side of the peak, and a CH_3 triplet (centered at δ 1.22). A striking feature of this figure is the pronounced influence of the electrolyte on the NH_3^+ and CH_2 resonances. The presence of NaCl causes an increase in the line width accompanied by a significant drop in peak intensities. The effect on line width is particularly pronounced above [NaCl] $\geq$ 0.1 *M*. At [NaCl] $\geq$ 0.35 *M*, the line broadening and the decreased intensity lead to complete disappearance of the absorption lines. Similar behavior was observed in DAC solutions for the addition of NaBr, $NaClO_4$, or $NaNO_3$. The effectiveness of the electrolyte anion in inducing changes in the appearance of the spectrum was found to increase in the order

$$Cl^- < NO_3^- = Br^- < ClO_4^- \quad (1)$$

Replacement of the protons of the quaternary ammonium head group (NH_3^+) by CH_3 groups does prevent the electrolyte effect. This is clearly shown in the ^1H spectrum for dodecyltrimethylammonium chloride (DTAC) which is not influenced by the presence of the salt.

In order to elucidate the factors controlling the observed spectral changes, spin–lattice relaxation times (T_1) were determined for the various types of protons and the results are summarized in Table II. It is noted that the T_1 value for the terminal methyl group decreases upon the formation of rods. This indicates longer correlation times (τ) for the motion which controls the relaxation process. It may seem surprising that the T_1 values for the methylene protons do not change significantly during the phase transition, while the line widths of peak undergo considerable broadening. However, this can be rationalized in terms of differences between the transverse and longitudinal relaxation times. Slower motion of the chains, e.g., segmental motions or rotations of the rods as a whole, are expected to decrease T_2 while T_1 may remain unaffected. As the line width is given by T_2, expressed by $\Delta\nu_{1/2} \geq (1/\pi T_2)$, then the line width increases during the phase transition despite the fact that T_1 remains unchanged. An alternative reason for the increase in line width can be sought in dipolar broadening. This phenomenon is caused by either slow isotropic motion or anisotropic motions which occur partially at a "slower rate".

Table II. Proton T_1 Values (sec) for Different Types of Protons in DAC Micellar Solutions in D_2O

Solution	$-CH_2-$	$-CH_3-$	$-NH_3^+$
DAC 0.1 *M*	0.470	0.87	0.65
DAC 0.1 *M* + NaCl 0.1 *M*	0.480	0.67	0.51
DAC 0.1 *M* + NaCl 0.2 *M*	0.475	0.545	0.52

Thus, significant changes occurring in the ^1HNMR spectra during the phase transition from spherical to rod-shaped micelles may be utilized to monitor the change. However, the information from proton T_1 values in these phase changes is not as significant. The line shape is a useful parameter to assess changes in the degree of association induced by the added electrolyte.[11] The relative efficiency of the added electrolyte in producing the phase transition may be interpreted in terms of the degree of hydrophobicity of the ions. Anions such as Br^- and ClO_4^- have a stronger hydrophobic character than Cl^- and hence display a greater affinity for adsorption in the Stern layer of cationic micelles.[6c,g,h] The binding of counterions neutralizes the surface charge promoting further aggregation. The strong interaction of the hydrophobic ions with the micellar surface is then responsible for the greater effectiveness of these ions in producing the sphere–rod phase transition.

Quite recently counterion binding to micelles has been studied in detail by calorimetric and potentiometric methods.[6i] The affinity of different ions for micellar surfaces is related to their position in the lyotropic series (Hoffmeister series).

The absence of line broadening in solutions of micellar DTAC emphasizes the role of the nature of the ionic head group in structural changes in solutions of cationic surfactants. DTAC molecules differ from DAC in that the protons of the ammonium groups are replaced by methyl groups. The presence of the methyl groups in the micellar surface layer apparently prevents the electrolyte-induced aggregation to larger micelles.

It should be emphasized that the ^1H CH_2 signal is an average comprised of contributions from 11 different methylene groups of the hydrocarbon chain. With ^{13}C NMR it is possible to detect the motions of the individual carbons forming the backbone of the surfactant molecule. As the chemical shifts for ^{13}C span a wider range ($\simeq$200 ppm), spin diffusion in natural abundance does not occur, so that the interpretation of T_1 measurements is simplified.

(2) ^{13}C NMR Investigations. The proton-decoupled ^{13}C NMR spectra of DAC (0.2 *M*) in spherical and rod-shaped micelles are presented in Figure 3. The spectrum consists of 9 resolved lines. The assignments for the lines are also given in the figure. In contrast to the proton spectrum the ^{13}C

Table III. ^{13}C Spin–Lattice Relaxation Times for DAC Micellar Solutions in D_2O

Solution	T_1, sec								
	C_{12}	C_{11}	C_{10}	C_9	C_8	C_7	C_{6-3}	C_2	C_1
0.2 DAC	2.23	0.96	0.82	0.53	0.41	0.47	0.485	0.46	0.37
0.2 DAC + 0.2 NaCl	2.20	1.12	0.65	0.33			0.38	0.46	0.45

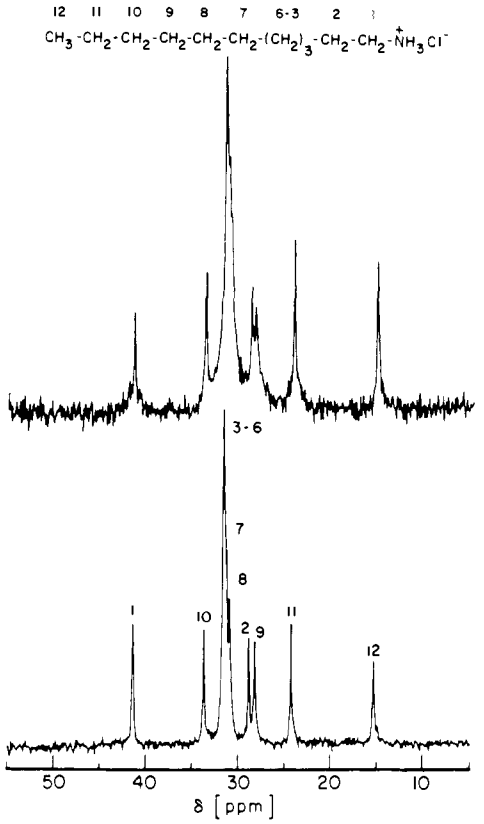

Figure 3. ^{13}C NMR spectrum of 0.2 *M* DAC solutions in D_2O in the absence (bottom) and in the presence (top) of 0.2 *M* NaCl.

spectrum retains the salient features of the spectrum in spherical aggregates, on addition of 0.2 *M* NaCl. There is a broadening of the base underneath the peaks, while the peak widths are affected differently by the electrolyte. For example, addition of NaCl narrows the C_1 peak while the other C_n peaks are unchanged or broadened. In Table III spin–lattice relaxation times (T_1) for the various resolved resonances are presented both in the absence and in the presence of 0.2 *M* NaCl. For a given shape of micelle, the T_1 values for individual carbon sites decrease with decreasing distance from the polar head group. The T_1 values for carbons 10 to 3 are smaller in the rod-shaped assemblies than in spherical aggregates, the T_1 values for C_{12} and C_{11} remaining unaffected.

In large and intermediate sized molecules the ^{13}C spin–lattice relaxation times[12] are dominated by ^{13}C–^1H dipolar interactions. For the simple case of a monoprotonated carbon the T_1 is related directly to the correlation time for the rotational reorientation of the pertinent C–H vector. Multiple-protonated carbons forming a long-chain molecule are subject to several internal rotational degrees of freedom in addition to the overall rotation of the molecule as a whole. In such cases an effective correlation time (τ_{eff}) is measured which is related to T_1 by

$$\frac{1}{T_1} = N\hbar^2\gamma_C^2\gamma_H^2 r_{CH}^{-6}\tau_{eff} \qquad (2)$$

where N is the number of directly attached protons, γ_H and γ_C are the gyromagnetic ratios of H and ^{13}C, respectively, $\hbar$ is Planck's constant, r_{CH} is the carbon–hydrogen bond length, and τ_{eff} is the effective correlation time.

If the overall reorientation of the micellized surfactant molecule is slow compared to the internal modes, then it is reasonable to assume that τ_{eff} is determined predominantly by the rotational mobility of individual protonated carbons. Thus T_1 values and their variations provide information about the relative mobility of a hydrocarbon chain in a given environment. In solutions of micellized DAC an increase in T_1 values is observed on moving from the polar head group toward the terminal CH_3, indicating a motional gradient along the chain with the CH_3 group being in a more fluid-like environment. This behavior parallels the earlier observations made in micellar solutions.[13] It should be noted, however, that the T_1 values for carbons 10 and above are considerably higher than those for the rest of the chain. Apparently, the most significant variation in microviscosity occurs in a narrow region of the micellar core. Addition of electrolyte causes two marked changes in the T_1 values: while the T_1 values for the backbone carbons decrease, the T_1 for α carbons increase. The first effect can be understood in terms of an increased rigidity of the environment of the hydrocarbon core, arising from a partial ordering of the hydrocarbon chains in the rod-like structure.[13a] Smaller T_1 values have also been observed for rod-shaped CTAB as compared with spherical *N*-octyltrimethylammonium bromide micelles. In order to explain the second phenomenon it is necessary to consider the effect of electrolyte on the structure of the micelle–water interface. It has been shown previously that the electrolytes may perturb the water structure surrounding the head groups and the adjacent methylene groups.[13b] A destruction of the water structure by the electrolyte ions present in the Stern layer of the rod-shaped aggregates may lead to greater freedom of motion for the α-CH_2 group.

It is still necessary to explain why the line widths of the carbon resonances do not show the dramatic increase upon the addition of electrolyte as is observed in the ^1H spectra. The T_1 values for the protons and carbons are comparable and cannot account for this effect. However, the T_2 for protons is expected to be shorter than for carbons, due to more efficient transverse relaxation resulting from the coupling of like spins (^1H···^1H) comparable to that of unlike spins. (^{13}C···^1H). Another[14] contribution to the shorter T_2 for protons could arise from intermolecular long-range dipolar interactions which are caused by slower motions of the surfactant molecules in the rods. The gyromagnetic ratio for ^1H is higher than for ^{13}C, and hence, ^1H is more susceptible to dipolar broadening.

Features of Pyrene Fluorescence in DAC Micellar Solutions

(1) Monomer and Excimer Fluorescence of Pyrene. The relatively long lifetime of the pyrene excited singlet state and its strong affinity for hydrophobic regions has prompted its use as a fluorescent probe for the hydrophobic regions of micelles and other biological macromolecules.[15] Another feature of this probe is the formation of excimers[16] which

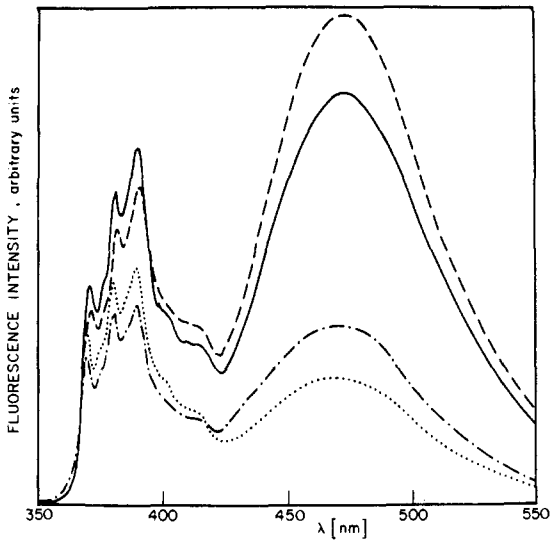

Figure 4. Fluorescence spectra of pyrene solubilized in 0.1 *M* DAC solutions, λ_{exit} 360 nm: (···) [pyrene] = 10^{-2} *M*; (-·-) [pyrene] = 10^{-3} *M*, [NaCl] = 0.2 *M*; (——) [pyrene] = 3×10^{-3} *M*, [NaCl] = 0.2 *M*; (---) [pyrene] = 3×10^{-3} *M*.

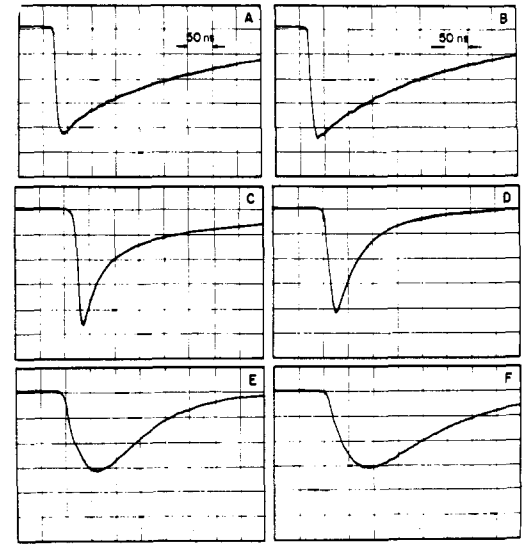

Figure 5. Decay of pyrene fluorescence (ordinate, relative fluorescence intensity) in spherical and rod-shaped micelles: A, [pyrene] = 10^{-4} *M*, λ 400 nm; B, [pyrene] = 10^{-4} *M*, [NaCl] = 0.2 *N*, λ 400 nm; C, [pyrene] = 10^{-3} *M*, λ 400 nm; D, [pyrene] = 10^{-3} *M*, [NaCl] = 0.2 *N*, λ 400 nm; E, [pyrene] = 5×10^{-4} *M*, λ 480 nm; F, [pyrene] = 5×10^{-4} *M*, [NaCl] = 0.2 *N*, λ 480 nm.

have a characteristic emission, red-shifted and easily separated from the monomer fluorescence.

$$P^* \xrightarrow{k_f} P \tag{3}$$

$$P^* + P \underset{}{\overset{k_e}{\rightleftharpoons}} P_2^* \tag{4}$$

$$P_2^* \xrightarrow[k_f']{} 2P \tag{5}$$

As the excimer formation of eq 4 occurs at a diffusion-controlled rate[17] the yield of excimer emission is sometimes correlated with the diffusion coefficient for pyrene within the investigated microenvironment.[18] The following section of data is concerned with a comparison of pyrene monomer and excimer fluorescence yields in spherical and rod-shaped DAC micelles. The results are supplemented by a kinetic analysis through the application of nanosecond laser photolysis. It will be shown presently that, in multiphase systems, the measurements of the pyrene monomer and excimer *yields alone* may not provide conclusive information about the diffusion rate of pyrene.

Figure 4 shows fluorescence spectra for pyrene dissolved in spherical and rod-shaped micelles. All four curves have the characteristic features of the pyrene fluorescence with the structured monomer emission peak in the 400-nm region and the broad structureless band of the excimer with a maximum around 480 nm. The ratio of the emission intensities at 480 and 400 nm, which is proportional to the excimer yield, is dependent on both pyrene concentration and the size of the micellar aggregate. In 10^{-3} *M* pyrene solution this ratio increases upon the addition of NaCl indicating a higher yield of pyrene excimers in rods. However, at 3×10^{-3} *M*, the electrolyte produces the reverse effect. Apparently at this probe concentration the excimer yield is higher in the spheres than in the rods. In order to interpret these data it is necessary to investigate the time dependency of monomer and excimer emission and to consider the distribution of pyrene in the micellar solutions. Oscilloscope traces showing the formation and decay of the pyrene monomer and excimer fluorescence in micellar DAC solutions are presented in Figure 5.

In *spherical aggregates*, the monomer fluorescence decay exhibits one smooth kinetic form up to a pyrene concentration of 10^{-4} *M*, and the fluorescence lifetime (τ_f) is 358

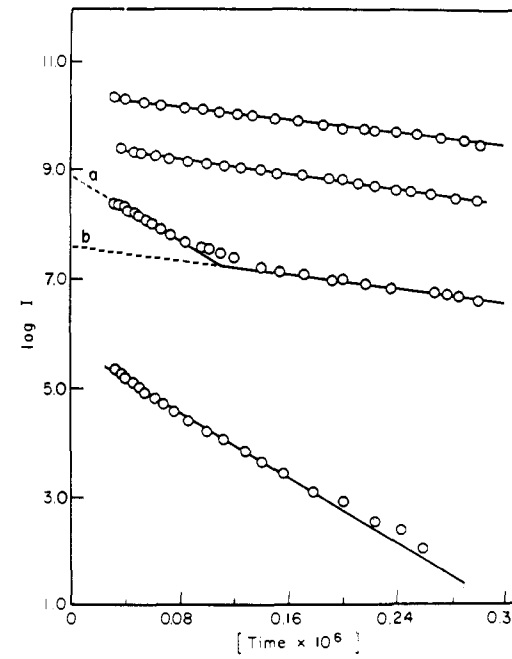

Figure 6. A semilogarithmic plot of intensity vs. time for the fluorescence decay curves shown in Figure 5. The form of plots (from the top) refer to the decay curves A, B, C, and D of Figure 5 respectively.

nsec. At higher pyrene concentrations the fluorescence curves consist of two parts: an initial steep decay followed by a slow component with a decay rate similar to that observed in dilute pyrene solutions. This behavior is more clearly demonstrated in Figure 6 which is a semilog plot of the monomer decay curves. The fraction of rapidly disappearing pyrene excited singlets (F) can be evaluated by extrapolating the two linear parts of a decay curve such as B back to the ordinate axis. From the intercepts a and b one obtains F via

$$F = 1 - e^{b-a} \tag{6}$$

The parameter F increases with increasing pyrene concentration. The rapid portion of the monomer decay is due to

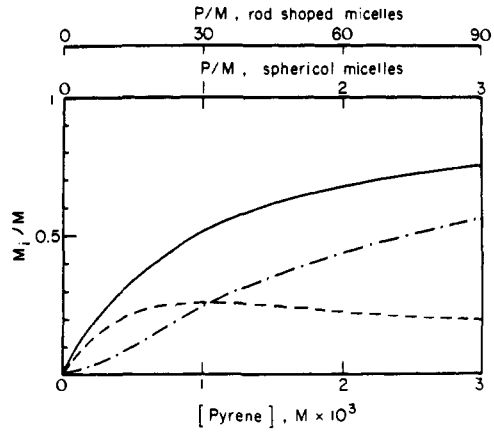

Figure 7. Distribution curves for pyrene in spherical and rod-shaped micellar solution, ordinate M_i/M (fraction of micelles occupied with i probe molecules): (---) $i = 1$, (-·-) $i > 1$, (——) $i \geq 1$. The average number of probes per micelle P/M was calculated from the concentration of micelles [M] and pyrene [P]. [M] = [(DAC) − (CMC)/n] where n, aggregation number, = 3000 for rods and 82 for spheres.

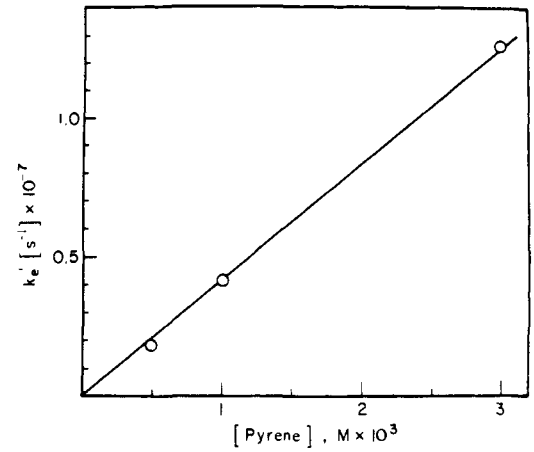

Figure 8. Effect of pyrene concentration on the specific rate of excimer formation in rod-shaped micelles.

excimer formation in micelles containing more than one pyrene molecule. This is amplified by the behavior of the excimer fluorescence, which is also shown in Figure 5. The growth of the excimer matches the initial fast monomer decay. A maximum is reached after ≃65 nsec. The subsequent decay, with $\tau_f = 70$ nsec, is typical of pyrene excimers in nonpolar environment. The specific rate for the excimer formation may be defined as

$$k_e' = (1/\tau_f - 1/\tau_f^0) \quad (7)$$

where τ_f and τ_f^0 are the lifetimes for the steep part of the monomer fluorescence decay and that in very dilute pyrene solutions, respectively. It was noted that k_e does not increase linearly with pyrene concentrations as would be expected if simple pseudo-first-order kinetics governed the excimer formation. For example, at [pyrene] = 10^{-3} M the slope of the steep linear part of the curve in Figure 5 gives $k_e' = 1.1 \times 10^7$ sec^{-1}, while $k_e' = 1.4 \times 10^7$ sec^{-1} at [pyrene] = 3×10^{-3} M.

In *rod-shaped* aggregates (0.1 M DAC, 0.2 M NaCl) the monomer fluorescence decay, at low pyrene concentration, is indistinguishable from that observed in spheres (Figure 5). A striking difference is noticeable, however, in solutions of pyrene $>10^{-4}$ M, where the decay is homogeneous and obeys first-order kinetics. At [pyrene] = 10^{-3} M the fluorescence decays more slowly than the initial fast part in solutions of spherical aggregates, but more rapidly than in dilute pyrene solutions. This indicates that the rate of excimer formation is decreased on forming rod structures from spherical micelles. The oscilloscope traces obtained at λ 480 nm confirm this statement. The excimer growth is slower and reaches a broad maximum after ≃80–100 nsec. The subsequent decay is also slower as compared to that observed in spherical aggregates. This is consistent with the kinetic scheme outlines in eq 3 to 5, as a decrease in the k_e value tends to broaden the excimer fluorescence curve. In rod-shaped aggregates the k_e' value increases linearly with pyrene concentration (Figure 7). Using the bulk pyrene concentration and the slope of the line, a k_e(rods) = 4.2×10^9 M^{-1} sec^{-1} is obtained. The pyrene concentration in the rods is about 30 times higher than the total bulk concentration, as the hydrocarbon phase in a 0.1 M DAC solution is only 3% of the total volume. Taking this into consideration a $k_e = 1.3 \times 10^8$ M^{-1} sec^{-1} is calculated.

It may be concluded that the yield of excimers formed in the two kinds of aggregates is determined by the rate of diffusion of pyrene molecules and the distribution of the probe among the micelles. If the surfactant is associated in relatively small spherical aggregates the degree of dispersity of the hydrocarbon microphase is high. Hence only a fraction of the micelles have more than one pyrene incorporated in them. This fraction alone will contribute to the excimer yield since the intermicellar exchange of pyrene is slow with respect to the excited state lifetime. Assuming a statistical distribution of the probes it is possible to derive values for the occupancy of spherical DAC micelles. These data are presented in Figure 8. These curves allow a prediction of the fraction of monomers decaying via excimer formation. For example, at 10^{-3} M pyrene, where the average concentration of pyrene per micelle is 1, 50% of the micelles are occupied. Half of these have two or more pyrene incorporated. Hence one expects that 50% ($F = 0.5$) of the fluorescence should decay rapidly via excimer formation as indeed is observed. Similar agreement with experimental parameter F was also found at other pyrene concentrations. These data vindicate the hypothesis that a statistical process controls the distribution of the probe in the micelles. In rod-shaped aggregates the average number of pyrene molecules per micelle is dramatically increased (Figure 8 second abscissa). At [pyrene] $\geq 10^{-4}$ M, almost all the rods will accommodate more than one probe. Hence here the statistical feature is much less important when considering excimer yields than in spherical aggregates. The controlling factor in the formation of excimers is via diffusion of the excited probe along the longitudinal axis, to a point where it eventually encounters another solubilized pyrene. The probability of encounter increases linearly with pyrene concentration and this explains the observed linear relation between k_e' and [pyrene]. From the rate constant $k_e = 1.2 \times 10^8$ M^{-1} sec^{-1} it is possible to derive that the rate of approach of the pyrene molecules within the rods is about a factor of 60 slower than in a normal hydrocarbon ($k_e = 7.0 \times 10^9$ M^{-1} sec^{-1}).[10] In spherically shaped micelles the diffusion is considerably faster than in the rods indicating that the sphere-rod transition is associated with an increase in microviscosity of the micellar interior. The slower rate of formation of excimer in these systems compared to simple liquid hydrocarbons reflects on the rate of lateral diffusion of pyrene and pyrene excited singlet states in the aggregates. Fluorescence polarization measurements give a measure of the rotational diffusion of the probe in aggregates. This effect will be dealt with further in connection with fluorescence depolarization measurements.

From Figure 4 it is possible to rationalize the two effects

of the electrolyte on the excimer yield at the two pyrene concentrations. In solutions with 10^{-3} M pyrene in spherical micelles the statistical effect plays a crucial role in the excimer formation process. Even though the rate of approach of two pyrene molecules in the rods is slower than in the spheres, a stronger excimer emission is found in the latter case. However, at 3×10^{-3} M pyrene the diffusion process predominates and leads to the inverse effect. It is believed that the above analysis may have significant bearing on the interpretation of similar experiments in more complex systems such as phospholipid dispersions, proteins, and biomembranes. In these systems the size and dispersity of the hydrophobic cavities (the site of optical probes such as pyrene) may control the distribution of the probe and hence complicate a simple interpretation of the fluorescence yields.

(2) Quenching of Pyrene Monomer Fluorescence. One point of particular interest in the properties of lipid–water interface is the permeability of the interface to different types of additives. Previous studies[6d] have established a correlation between the rate of fluorescence quenching of the solubilized probe and the ease of access of a quencher (which may mainly dissolve in the aqueous phase) to the solubilization site. This can be made use of to test the permeability changes during the sphere–rod transitions in DAC solutions. Such experiments are preferably performed at low pyrene concentrations [(pyrene) $\leq 10^{-4}$ M] in order to avoid excimer formation. Under these conditions, the quenching efficiency is given by

$$k = k_0 + k_q[Q] \tag{8}$$

where k = the observed rate constant, k_0 = the rate constant of the fluorescence decay in the absence of quencher, k_q = the quenching efficiency, and [Q] = the concentration of the quencher.

Table IV summarizes the data obtained from laser photolysis studies of pyrene monomer fluorescence in the presence of various ionic and nonionic quenchers. For cations such as Tl^+ and Cu^{2+} the rate constants obtained for the micellar solutions are markedly lower than the quenching efficiency in methanol; thallous ion shows a relatively higher efficiency than Cu^{2+}. The k_q values for both ions increase when rod-shaped aggregates are present. The reverse effect is shown by the iodide ions. The quenching rate constant for spherical micelles in even greater than in homogeneous solution and decreases on forming rod-like structures. Finally the quenching reaction of oxygen is slightly faster in rods than in spherical micelles but considerably slower than in methanol.

In principle the ease of entry of a quencher from an aqueous environment into a micelle can be influenced by four factors: the charge of the interface, the charge of the ion, the separation of the head groups, and the microviscosity of the micellar interior. The present data exemplify this concept. Clearly, in the case of a cationic quencher the electrostatic repulsion at the micellar surface prevents its approach to pyrene in the micelle and hence reduces the probability of quenching. This effect is less pronounced in rod-shaped micelles as the surface potential decreases upon the addition of the electrolyte. Copper ions being doubly charged are subject to stronger repulsion forces which explains the observed differences in the k_q values. Similarly, the attraction of the I^- toward the charged interface leads to an enhanced quenching efficiency in the spherical micelles compared to that in methanol or in rods. At first sight it is surprising that oxygen can penetrate the rods more readily than the spherical micelles, as the micellar head groups are expected to be more closely packed in the large aggregate.[19] Presumably, the added NaCl in the former solution disrupts the water structure around the head groups in the interface which could offset this effect.

Table IV. Summary of Pyrene Fluorescence Quenching Efficiency in Solutions of Spherical and Rod-Shaped DAC Micelles

Quencher	k_q(sphere), M^{-1} sec^{-1}	k_q(rod), M^{-1} sec^{-1}	k_{CH_3OH}, M^{-1} sec^{-1}
Tl^+	3.1×10^7	3×10^8	5×10^9
Cu^{2+}	$<10^6 M^{-1}$ sec^{-1}	4.6×10^7	2×10^{10}
I^0	6×10^9	2.5×10^9	3×10^9
O_2	3.5×10^9	4.3×10^9	2×10^{10}

A special situation arises if the quencher is an ion such as Br^- which specifically binds to the surface of a micelle. This case has been dealt with previously in the interpretation of pyrene fluorescence data in CTAB micellar solutions.[6c] A similar consideration applies for the solutions of DAC containing pyrene as a fluorescent probe and an excess of Br^- electrolyte. Equation 8 no longer describes the quenching kinetics since the decay of pyrene monomer fluroescence is controlled by the fraction of micellar surface covered with Br^- ions and the rate of diffusion of pyrene excited state toward micelle–water interface. In solutions containing 0.2 M NaBr, 0.05 M DAC, and 10^{-5} M pyrene the fluorescence lifetime (τ_f) is 200 nsec. Increasing the [Br^-] to 0.3 M reduces T_f to 180 nsec. It was pointed out in the NMR section that NaBr induces a phase transition and that rod-shaped aggregates of DAC prevail at [NaBr] $\geq$ 0.1 M. The above data may then be interpreted in terms of radial diffusion of pyrene from the center to the surface of the rods. The quenching efficiency of NaBr can be expressed as

$$k_q = 1/\tau - 1/\tau_0 \tag{9}$$

where τ_0 is the lifetime of pyrene in rod-shaped micelles with Cl^- counterions. The data give $k_a = 2.17 \times 10^6$ sec^{-1} at 0.2 M NaBr and $k_q = 2.72 \times 10^6$ sec^{-1} as 0.3 M NaBr. At 0.3 M NaBr most of the surface is expected to be occupied with Br^- ions. Hence, the latter k_q value is determined predominantly by the diffusion of pyrene to the surface. Hence, the diffusion of pyrene excited state from the interior to the surface of the rod has a $t_{1/2} \simeq 254$ nsec. This value is considerably higher than $t_{1/2} = 90$ nsec found for the diffusion in spherical CTAB micelles[6c] indicating greater obstruction for the radial diffusion in the larger aggregates.

(3) Fluorescence Depolarization Studies in DAC/NaCl Micellar Solutions. A direct and convenient method to observe restrictions on molecular motions is through the study of depolarization of fluorescence. In solutions of fluorescent molecules the degree of polarization of the emitted light measured at right angles on the incident polarized light beam is given by the Perrin equation[20]

$$\left(\frac{1}{P} - \frac{1}{3}\right) \Big/ \left(\frac{1}{P_0} - \frac{1}{3}\right) = 1 + \frac{kT\tau}{\eta v_0} \tag{10}$$

where P = the degree of polarization in the given solution, P_0 = the degree of polarization measured in an extremely viscous solvent, k = the Boltzmann constant, τ = the average lifetime of the probe molecule in the excited state, η = the viscosity, T = the temperature in °K, and v_0 = the effective volume. Thus the parameter P is related to the viscosity in the immediate environment of the probe. Measurements of the degree of polarization were carried out with solutions labeled with 2-methylanthracene (MA) or 1-anilino-8-naphthalenesulfonate (ANS), used as fluorescent probes in 0.1 M DAC solutions in the presence of various

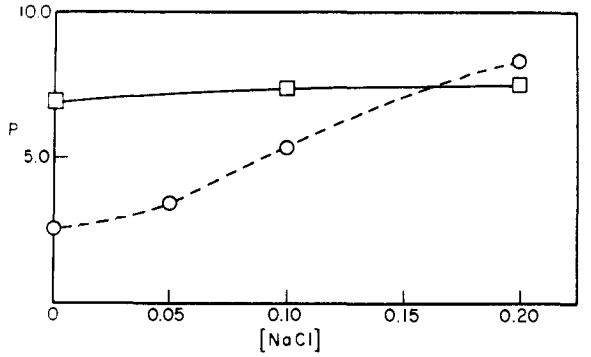

Figure 9. Effect of NaCl electrolyte on the degree of polarization of 2-methylanthracene (4×10^{-6} *M*) and 1-anilino-8-naphthalenesulfonate (2×10^{-6} *M*) in 0.1 *M* DAC solution.

concentrations of electrolyte. Figure 9 shows changes in the parameter *P* occurring during the electrolyte-induced phase transition.

A significant increase of *P*, measured at 40°, is observed for 2-methylanthracene when the micellar organization changes from a sphere to a rod-like structure. It may safely be assumed that the fluorescence lifetime of the probe does not differ significantly in the two forms of the aggregates. Hence, it may be concluded that the formation of larger aggregates is accompanied by a marked increase in the microviscosity. This indicates a smaller mobility and therefore a tighter packing of the surfactant chain molecules. This inference of tighter packing in the rod-shaped micelle is in agreement with the NMR measurements which were discussed above. Such restrictions in the micelles may originate from the fact that the surfactant head groups are more closely spaced in the rods than in the spherical micelles.

In contrast to the results obtained with 2-methylanthracene the use of ANS does not reveal significant changes in the degree of polarization during the phase transition, Figure 9. This behavior can be rationalized in terms of different solubilization sites for the two probes. Whereas 2-methylanthracene residues in the hydrophobic interior of the micellar aggregates, the ANS is expected to be located at the micelle-water interface. The negative sulfonate of the ANS, similar to pyrenesulfonic acid or arylsulfonates[21] in general, is associated preferably with the cationic head group of the micellar surfactant molecules.

Conclusions

NMR and photochemical studies may be employed to probe in detail the physical properties of various forms of aggregates present in solutions of amphiphilic molecules. Significant alterations occurring during transitions among the different structural organizations can be detected. NMR line shape and relaxation measurements performed with aqueous DAC solutions reveal changes in the segmental mobility of different regions of the hydrocarbon chains upon the electrolyte-induced transition of spherical micelles into rod-like structures. The slower segmental motions occurring in the latter are associated with an increase in the microviscosity of hydrocarbon interior. The differences in the architecture of these micellar assemblies lead to unique photochemical consequences. For example, the yield of excimers of photoactive probes and their rate of formation are greatly affected by the size of the aggregates. The investigated systems are suitable models for more complex forms of bioaggregates. The present studies clearly demonstrate the scope and limitations of the techniques which are frequently employed in these situations.

Acknowledgment is made to the donors of the Petroleum Research Fund, admininstered by the American Chemical Society, for partial support of this research.

References and Notes

(1) The Radiation Laboratory of the University of Notre Dame is operated under contract with the U.S. Atomic Energy Commission. This is AEC Document No. C00-38-974.
(2) (a) E. H. Cordes, "Reaction Kinetics in Micelles", Plenum Press, New York, N.Y., 1973; (b) E. H. Cordes and C. Gitler, *Prog. Bioorg. Chem.*, **2**, 1 (1973); (c) C. Tanford, "The Hydrophobic Effect; Formation of Micelles and Biological Membranes", Wiley-Interscience, New York, N.Y., 1973.
(3) E. J. Fendler and J. H. Fendler, *Adv. Phys. Org. Chem.*, **66**, 1472 (1970).
(4) (a) J. C. Eriksson and G. Gillberg, *Acta Chem. Scand.*, **20**, 2019 (1966); (b) J. Clifford and B. A. Pethica, *Trans. Faraday Soc.*, **61**, 182, (1965); J. Clifford, *Ibid.*, **61**, 1276 (1965); (c) E. J. Fendler, C. L. Day, and J. H. Fendler, *J. Phys. Chem.*, **76**, 1460 (1972); (d) N. Muller, ref 2a, p 1.
(5) (a) M. J. Povich, J. A. Mann, and A. Kawamato, *J. Colloid Interface Sci.*, **41**, 145 (1972); (b) J. Oakes, *J. Chem. Soc., Faraday Trans. 2*, **69**, 1321 (1973). (c) N. M. Atherton and S. J. Strach, *J. Chem. Soc., Faraday Trans. 2*, **68**, 374 (1972); (d)A. S. Waggoner, O. H. Griffith, and C. R. Christensen, *Proc. Natl. Acad. Sci. U.S.*, **57**, 1198 (1967).
(6) (a) G. Weber, *Annu. Rev. Biophys. Bioeng.*, **1**, 553 (1972); (b) S. C. Wallace and J. K. Thomas, *Radiat. Res.*, **54**, 49 (1973); (c) M. Grätzel and J. K. Thomas, *J. Am. Chem. Soc.*, **95**, 6885 (1973); (d) P. P. Infelta, M. Grätzel, and J. K. Thomas, *J. Phys. Chem.*, **78**, 190 (1974); (e) M. Chen, M. Grätzel, and J. K. Thomas, *Chem. Phys. Lett.*, **24**, 65 (1974); (f) H. J. Pownall and L. C. Smith, *J. Am. Chem. Soc.*, **95**, 3136 (1973); (g) R. R. Hautala, N. E. Schore, and N. J. Turro, *J. Am. Chem. Soc.*, **95**, 5508 (1973); (h) L. K. Patterson and E. Viel, *J. Phys. Chem.*, 77, 1191 (1973); (I) J. W. Larsen and L. J. Magid, *J. Am. Chem. Soc.*, **96**, 5774 (1974).
(7) P. A. Winsor, *Chem. Rev.*, **68**, 1 (1968).
(8) (a) L. M. Kushner, W. D. Hubbard, and R. A. Parker, *J. Res. Natl. Bur. Stand.*, 113 (1957). (b) M. F. Emerson and A. Holtzer, *J. Phys. Chem.*, **71**, 1898 (1967); (c) I. Cohen and T. Vassillades, *Ibid.*, **65**, 1774 (1961); (d) K. D. Lawson and T. J. Flautt, *Ibid.*, **72**, 2066 (1968); (e) P. Debye and E. W. Anacker, *Ibid.*, **55**, 644 (1951); (f) K. W. Hermann, *Ibid.*, **68**, 1540 (1964); (g) E. W. Anacker, *Ibid.*, **62**, 41 (1958).
(9) R. Freeman and H. D. W. Hill, *J. Chem. Phys.*, **54**, 3367 (1971).
(10) (a) R. McNeil, J. T. Richards, and J. K. Thomas, *J. Phys. Chem.*, **74**, 2290 (1970); (b) G. West, J. T. Richards, and J. K. Thomas, *Ibid.*, **74**, 4137 (1970).
(11) (a) C. A. Bunton and M. J. Minch, *J. Phys. Chem.*, **78**, 1490 (1974); (b) C. A. Bunton, M. J. Minch, J. Hidalgo, and L. Sepulveda, *J. Am. Chem. Soc.*, **95**, 3262 (1973).
(12) D. Doddrell, V. Glushko, and A. Allerhand, *J. Chem. Phys.*, **56**, 3683 (1972).
(13) (a) E. Williams, B. Sears, A. Allerhand, and E. H. Cordes, *J. Am. Chem. Soc.*, **95**, 4871 (1973); (b) R. T. Roberts and C. Chachaty, *Chem. Phys. Lett.*, **22**, 348 (1973); (c) G. C. Levy, R. A. Komoroski, and J. A. Halstead, *J. Am. Chem. Soc.*, **96**, 5456 (1974).
(14) A. Abragam, "The Principles of Nuclear Magnetism", Oxford University Press, London, 1961.
(15) (a) Th. Forster and B. Selinger, *Z. Naturforsch., Teil A*, **19**, 39 (1964); (b) H. J. Pownall and L. C. Smith, *Biochemistry*, **13**, 2590 (1974); (c) H. C. Pownall and L. C. Smith, *ibid.*, **13**, 2594 (1974); (d) S. Cheng, J. K. Thomas, and C. F. Kulpa, *ibid.*, **13**, 1135 (1974).
(16) Th. Forster, *Angew. Chem., Int. Ed. Engl.*, **8**, 333 (1969).
(17) J. B. Birks and H. Munro, *Prog. React. Kinet.*, **4**, 239 (1967).
(18) (a) A. K. Soutar, H. J. Pownall, A. S. Hu, and L. C. Smith, *Biochemistry*, **13**, 2828 (1974); (b) H. J. Galla and E. Sackmann, *Biochem. Biophys. Acta*, **339**, 103 (1974).
(19) (a) C. Tanford, *J. Phys. Chem.*, **76**, 3020 (1972); (b) C. Tanford, *Proc. Natl. Acad. Sci. U.S.*, **71**, 1811 (1974).
(20) F. Perrin, *Ann. Phys. (Paris)*, **17**, 283 (1932).
(21) C. A. Bunton, ref 2a, p 73.